INTERNATIONAL JOURNAL FOR NUMERICAL METHODS IN FLUIDS, VOL. 19, 321–342 (1994)

SIMULATION OF THREE-DIMENSIONAL UNSTEADY VISCOUS FREE SURFACE FLOW AROUND A SHIP MODEL

B. ALESSANDRINI AND G. DELHOMMEAU

Division Hydrodynamique Navale, Laboratoire de Mécanique des Fluides, URA 1217 CNRS, Ecole Centrale de Nantes, 1 Rue de la Noë, F-44072 Nantes Cedex 03, France

SUMMARY

We present here a numerical method for solving the free surface flow around a ship at forward speed in calm water. The fluid is assumed to be Newtonian and the Reynolds-averaged Navier–Stokes equations are solved by a finite difference method. Modelization of turbulence is achieved by the algebraic model proposed by Baldwin and Lomax. Fully non-linear free surface conditions are satisfied in the model and a method to avoid the incompatibility between free surface conditions and no-slip conditions at the waterline is proposed. Numerical results obtained for a Wigley hull are compared with experimental results.

KEY WORDS Navier–Stokes equations Free surface flow Finite difference Wave resistance Frictional resistance Adaptive mesh

1. INTRODUCTION

The standard approach to the numerical study of incompressible flow around the hull of a boat may be divided into two distinct methods; either the irrotational perfect fluid hypothesis is chosen and the problem is solved by a panel method with linear or non-linear free surface conditions[1,2] or the fluid viscosity is taken into account and the Reynolds-averaged Navier–Stokes equations are solved with or without simplification (Navier–Stokes parabolized equations, boundary layer equations) for the double model only (without any free surface condition).[3–5]

In the first method the wave elevation around the hull with forward speed and therefore its wave resitance can be calculated in accordance with the solution of the perfect fluid problem, which varies according to the Froude number only. The flow separation at the stern of the boat, the velocity profile in the boundary layer and frictional and form resistances cannot be obtained by this theory and seem to be particular to the second method. However, in the second method the wave elevation and consequently the wave resistance cannot be obtained.

All the components of the ship resistance can be obtained by using two computer codes, based on both theories previously mentioned, with the hypothesis of uncoupling gravity forces and viscous forces, which is not easily controllable.

The success of this method is largely due to the validity of Froude's hypothesis, which supposes that for realistic scales and for boats with smooth shapes the problem of wave resistance is not quite coupled with the viscous problem. Thus it seems possible to consider as a first approxima-

CCC 0271–2091/94/160321–22

Received February 1993
Revised February 1994

tion that the wave resistance essentially varies according to the Froude number and the frictional resistance according to the Reynolds number.

This approximation fails as soon as viscous effects appear near the free surface (thickening of the boundary layer at the stern, separation, etc.). In this case an important dependence of the wave elevation on the Reynolds number and of the velocity profile in the boundary layer on the Froude number is to be noted.

The first-order boundary layer equations present an attractive option for this problem, because viscous effects are naturally coupled with the perfect fluid. It can be shown that linear free surface conditions in the pressure field calculation (perfect fluid) are consistent with the boundary layer hypothesis. A weak coupling with transpiration velocities is an interesting alternative in order to take into account the boundary layer effects in the free surface perfect fluid calculation. Unfortunately, obtaining convergence of the process for low Reynolds numbers remains difficult and we come up against problems that are particular to the weak coupling formulation: the impossibility of calculating flow separation and the indetermination of the results concerning local parameters for concave geometry.[6]

For all these reasons numerical solutions of the full Navier–Stokes equations with free surface conditions appear today.[7]

A finite difference formulation to solve the Reynolds-averaged Navier–Stokes equations for the calculation of three-dimensional turbulent viscous incompressible flow past a ship hull with forward speed in the presence of a free surface is presented in this paper.

Writing the equations in a Cartesian system[8] (e.g. the Tummac formulation) reveals some problems in taking into account no-slip conditions on the body and viscous free surface boundary conditions: sufficient refinement of the mesh in order to obtain a good description of the velocity profile in the boundary layer, especially for high Reynolds numbers, is not possible. In consequence, the integration of the stress on the hull grid is very imprecise and the prediction of resistance is poor. In this paper the unsteady Navier–Stokes equations written in a conforming curvilinear grid system will be used so that the body and the free surface will describe co-ordinate surfaces at each time step.[7]

The independent unknowns are the three Cartesian components of physical velocity, pressure and wave elevation on the free surface. A partial transformation of the equations will be used.

Closure of the equations is realized by an algebraic turbulence model (Baldwin–Lomax or Cebeci–Smith) without a wall function. By this approach the real performances of the model can be tested, but this requires a very fine meshing around the body and a preconditioning of linear systems.

Fully viscous free surface conditions are written for the real position of the boundary. The kinematic condition is used for the calculation of the new free surface elevation at the end of each iteration. The normal dynamic condition is taken into account as a Dirichlet condition on the pressure and both tangential dynamic conditions are taken into account as Neumann conditions on velocities. Unfortunately, free surface conditions are inconsistent with boundary conditions on the body:[9,10] no-slip conditions inhibit numerically the motion of the free surface along the hull and induce too important stress in the dynamic condition. A relaxation method of the free surface boundary conditions near the body is used to solve the problem numerically.

After the presentation of the flow equations a general method of numerical resolution is proposed for the conforming griding, for the discretization of the transport equation of the mean momentum, for the discretization of the continuity equation, for the resolution of linear systems and the preconditioning and for the discretization of the free surface boundary conditions.

2. EQUATIONS

2.1. *Primitive form*

The Navier–Stokes equations are written in the so-called Galilean orthogonal system (x^1, x^2, x^3). The independent unknowns are the Cartesian components of the mean physical velocity, (u^1, u^2, u^3), and the mean pressure P. Gravity forces, which are needed for calculation with a free surface, are taken into account by the change of variable $p = P + \rho g x^3$. A Newtonian closure for Reynolds stresses using a turbulent viscosity ν_t and the kinetic energy of turbulence, k, is employed. The fluid is assumed to be incompressible.

$$\frac{\partial u^\alpha}{\partial t} + u^j \frac{\partial u^\alpha}{\partial x^j} = -\frac{1}{\rho}\frac{\partial p}{\partial x^\alpha} + \nu \frac{\partial^2 u^\alpha}{(\partial x^j)^2} - \frac{\partial}{\partial x^j}(\overline{u'^\alpha u'^j}),$$

$$\overline{u'^i u'^j} = \tfrac{2}{3} k \delta_{ij} - \nu_t \left(\frac{\partial u^i}{\partial x^j} + \frac{\partial u^j}{\partial x^i}\right), \qquad \frac{\partial u^i}{\partial x^i} = 0. \tag{1}$$

2.2. *Computational box*

The physical domain in which the flow is calculated is limited by the unstream input plane, the downstream output plane, the hull, its symmetry plane and the free surface. A transformation of the boundary conditions on the hull and the free surface is induced by using curvilinear co-ordinates. The physical domain is transformed into a computational box in which the free surfaces and the hull are planes. The directions ε^1, ε^2 and ε^3 are shown in Figure 1.

The partial transformation consists of using Cartesian components of the velocity which vary according to the ε^i-co-ordinates. The total transformation, which would require the calculation of third-order metric coefficients (Christoffel coefficients), will not be used. The Navier–Stokes equations with partial transformation are

$$\frac{\partial u^\alpha}{\partial t} = \nu g^{ij} \frac{\partial^2 u^\alpha}{\partial \varepsilon^i \partial \varepsilon_j} - \left(\frac{1}{J} b_j^i (u^i - v_g^i) - \nu f^j\right) \frac{\partial u^\alpha}{\partial \varepsilon^j} - \frac{1}{\rho J} b_\alpha^k \frac{\partial p}{\partial \varepsilon^k} - \frac{1}{J} b_j^k \frac{\partial}{\partial \varepsilon^k}(\overline{u'^\alpha u'^j}),$$

$$\overline{u'^i u'^j} = \tfrac{2}{3} k \delta_{ij} - \frac{\nu_t}{J}\left(b_j^k \frac{\partial u^i}{\partial \varepsilon^k} + b_i^k \frac{\partial u^j}{\partial \varepsilon^k}\right), \qquad \frac{1}{J} b_j^i \frac{\partial u^i}{\partial \varepsilon^j} = 0. \tag{2}$$

The particularity of a calculation with free surface boundary conditions is the evolution of the physical space while the calculation space is fixed. The metric which is applicable to each iteration for the transformation consists of the Jacobian J, the covariant basis a_i, the oriented

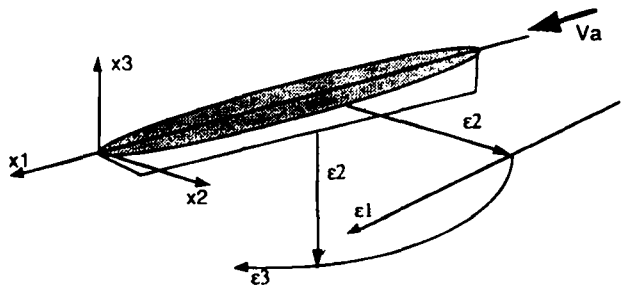

Figure 1

area vectors b^j, the contravariant metric tensor g^{ij}, the grid control parameters f^i and the displacement velocity of the mesh, v_g:

$$a_{ij} = \frac{\partial x^j}{\partial \varepsilon^i}, \qquad J = \det(a_{ij}), \qquad b^i = a_i \wedge a_k (i, j, k) \text{ cyclic},$$
$$g^{kl} = \frac{1}{J^2} b^k_j b^l_j, \qquad f^k = \frac{1}{J} \frac{\partial (J g^{ik})}{\partial \varepsilon^l}, \qquad v^i_g = \frac{\partial x^i}{\partial t}. \tag{3}$$

2.3. *Turbulence model*

When calculating realistic flows around a real ship, the Reynolds numbers are about 10^8 or 10^9, and 10^6 or 10^7 for a model: therefore turbulence equations have to be used. The turbulent viscosity, introduced by the Newtonian closure which links the Reynolds stress to the mean velocity field, is expressed by a turbulence model and the influence of the turbulent kinetic energy (k) is included in the pressure term ($p + \frac{2}{3}\rho k$). The calculation has been done with an algebraic model based on a mixing length formulation adapted for Navier–Stokes computation by Baldwin and Lomax.[11] This model is used with a damping function of Van Driest (F_{vd}) but without a wall function. The normal distance (d) from the grid point to the body is obtained by calculating the curvilinear abscissa along the ε^2-line of the mesh. In the wake we consider the distance from the grid point to the symmetry plane ($y = 0$) and the damping function of Van Driest is not used.

The Degani–Schiff correction is satisfactory for the double model, but the free surface conditions induce irregularities in the calculation of the frontier of external and internal domains and subsequently in the calculation of the turbulent viscosity. This numerical problem is avoided by restricting the search of the froniter, i.e. the search of the maximum of the function $d\omega F_{vd}$ along the ε^2-line, to the boundary layer instead of considering the whole profile which extends from the hull to the exterior boundary of the calculation domain. In this model free surface effects are not modelized and ω represents the modulus of the rotation of the flow.

2.4. *The free surface boundary conditions*

The free surface boundary conditions consist of one kinematic condition and three dynamic conditions.

The kinematic condition ensures that the fluid particles of the free surface stay on the free surface at any time. If h is the free surface elevation, this condition is written as $Dh/Dt = u^3$ or in Cartesian co-ordinates as

$$\frac{\partial h}{\partial t} + u^1 \frac{\partial h}{\partial x} + u^2 \frac{\partial h}{\partial y} = u^3. \tag{4}$$

The dynamic conditions represent the continuity of stress on the free surface. In the perfect fluid approximation only the continuity of the normal component, which is the pressure, is assumed, but in a viscous fluid the tangential stress has to be taken into account. The continuity of normal stress is then no longer the continuity of pressure, and viscous terms and turbulent terms must be used.

The stress tensor is

$$\sigma_{ij} = (-\tfrac{2}{3}\rho k - P)\delta_{ij} + \rho \nu_e \left(\frac{\partial u^i}{\partial x^j} + \frac{\partial u^j}{\partial x^i} \right). \tag{5}$$

The ith component of the stress on the free surface is

$$T_i = \left[(-\tfrac{2}{3}\rho k - p + \rho g x^3)\delta_{ij} + \rho \nu_e \left(\frac{\partial u^i}{\partial x^j} + \frac{\partial u^j}{\partial x^i} \right) \right] b_j^3. \tag{6}$$

Therefore the normal stress component on the free surface is obtained as

$$T_n = \left[(-\tfrac{2}{3}\rho k - p + \rho g x^3)\delta_{ij} + \rho \nu_e \left(\frac{\partial u^i}{\partial x^j} + \frac{\partial u^j}{\partial x^i} \right) \right] \frac{b_j^3 b_i^3}{|b^3|} \tag{7}$$

and the normal dynamic condition in Cartesian co-ordinates is

$$\left[\mathrm{p} - \tfrac{2}{3}\rho k - p + \rho g x^3)\delta_{ij} + \rho \nu_e \left(\frac{\partial u^i}{\partial x^j} + \frac{\partial u^j}{\partial x^i} \right) \right] \frac{b_j^3 b_i^3}{|b^3|} = \frac{\gamma}{r_1 + r_2}, \tag{8}$$

where γ is the surface tension coefficient and r_1 and r_2 are the two principal curvature radii of the free surface.

Taking into account $a_\alpha b^3 = 0$ ($\alpha = 1$ or 2) on the free surface, the continuity of tangential stress in Cartesian co-ordinates is written as

$$T_{t_\alpha} = 0 \quad \Leftrightarrow \quad \left(\frac{\partial u^i}{\partial x^j} + \frac{\partial u^j}{\partial x^i} \right) b_j^3 a_{\alpha i} = 0. \tag{9}$$

A partial transformation whereby Cartesian co-ordinate equations are transformed into curvilinear co-ordinates equations in the computational space is applied to the previous equations. The kinematic, normal dynamic and tangential dynamic conditions are respectively

$$\begin{gathered} \left(\frac{\partial h}{\partial t} + \frac{1}{J} b_i^j (u^i - v_g^i) \frac{\partial h}{\partial \varepsilon^j} \right) - u^3 = 0, \\ p = \rho g h - \tfrac{2}{3}\rho k + \frac{2\rho \nu_e}{J|b^3|^2} b_i^3 b_j^3 b_i^k \frac{\partial u^i}{\partial \varepsilon^k} + \frac{\gamma}{(r_1 + r_2)|b^3|}, \\ (b_j^k b_j^3 a_{\alpha i} + b_j^k b_i^3 a_{\alpha j}) \frac{\partial u^i}{\partial \varepsilon^k} = 0. \end{gathered} \tag{10}$$

3. NUMERICAL RESOLUTION

3.1. Meshing

The convergence to a steady state is obtained by a time step method. At the end of each time step a new free surface is computed and a new mesh is fitted to the physical space. The meshing method takes a lot of CPU time if it is used at each time step. A numerically faster meshing scheme is proposed here.

An initial structured monoblock mesh is computed by a method of transfinite interpolation.[12] This mesh is fitted on the upstream and downstream planes and on the body which has been first discretized above the assumed final location of the free surface.

The numerical method has been developed for general non-orthogonal grids, but an orthogonalization of the mesh ensures a better accuracy in the calculation of the metric coefficients, so the mesh is orthogonalized as far as possible by adding conditions on the direction of the grid

lines of the boundaries of the domain. The concentration of the grid around the body can be adapted by a control function in order to have a precise computation of the velocity in the boundary layer (the mesh is refined on the bow of the boat because of the boundary layer thinness). Finally the mesh is smoothed in order to restrain the propagation of the discontinuity of the first derivative at the intersection of hull and symmetry plane along grid lines (the transfinite interpolation method expands the drawback of the mesh).

This initial mesh is used for all re-gridding operations at each time step. The method is the following. The initial mesh has to be cut by the free surface while maintaining the structural character of the mesh and the number of grid lines in each direction ($\varepsilon^1, \varepsilon^2, \varepsilon^3$). Each grid line which starts at the free surface (ε^3 grid line) is considered independently and the points are distributed according to the new free surface elevation. On each line the same curvilinear abscissa is preserved and the refinement of the mesh is kept.

The advantage of this method is its low CPU time. In return the orthogonality of the mesh is lost.

The independent unknowns (velocities u^i, pressure p and free surface elevation h) are located at the nodes of the grid (node-centred disposition).

3.2. *Discretization*

3.2.1. Continuity equation. The discretization of the continuity equation uses nine first-order derivatives on velocities (each component of the velocities in the three directions of the mesh). For numerical calculation a classical centred scheme with seven nodes can be used. This method is accurate to second order and does not require interpolation for a node-centred disposition, but is sensitive to the problem of odd and even uncoupling. Therefore a first-order-accurate non-centred scheme with four points is preferred. This scheme, being used with an opposite non-centred discretization of the pressure gradient in the three directions, gives a discretization of the pressure equation with 13 points, which produces a better conditioning of the pressure matrix.

3.2.2. Momentum equation. Using the change of variable $\varepsilon^{i*} = \varepsilon^i/(g^{ii})^{0.5}$, the transport equation for the mean momentum is written in the linearized form

$$\Phi_{\varepsilon^{1*}\varepsilon^{1*}} + \Phi_{\varepsilon^{2*}\varepsilon^{2*}} + \Phi_{\varepsilon^{3*}\varepsilon^{3*}} = 2A\Phi_{\varepsilon^{3*}} + 2B\Phi_{\varepsilon^{2*}} + 2C\Phi_{\varepsilon^{1*}} + D\Phi_t + S_\Phi, \tag{11}$$

where Φ is one of the three components of the mean velocity and the convection terms A, B and C and source terms S_Φ are calculated at the previous time step. The discretization is made only on the first- and second-order derivative terms in ε^{i*}. In order to limit the numerical diffusion and to obtain continuous discretization coefficients with convection velocities, analytical discretization schemes have been tested, being considered as more accurate than an upwind finite difference scheme.

A bidimensional finite analytic scheme (Figure 2) was first tried, associated with an uni-exponential scheme in the third direction. This method is based on the following decomposition of the transport equation:

$$\Phi_{\varepsilon^{2*}\varepsilon^{2*}} + \Phi_{\varepsilon^{3*}\varepsilon^{3*}} - 2B\Phi_{\varepsilon^{2*}} - 2A\Phi_{\varepsilon^{3*}} = g, \qquad -\Phi_{\varepsilon^{1*}\varepsilon^{1*}} - 2C\Phi_{\varepsilon^{1*}} + D\Phi_t + S_\Phi = g. \tag{12}$$

The discretization of the first equation is achieved by the finite analytic method carried out by Chen and Chen:[13,14] a nine-node bidimensional grid is used and it is assumed that the boundary conditions on the four sides of the grid are given by linear combinations

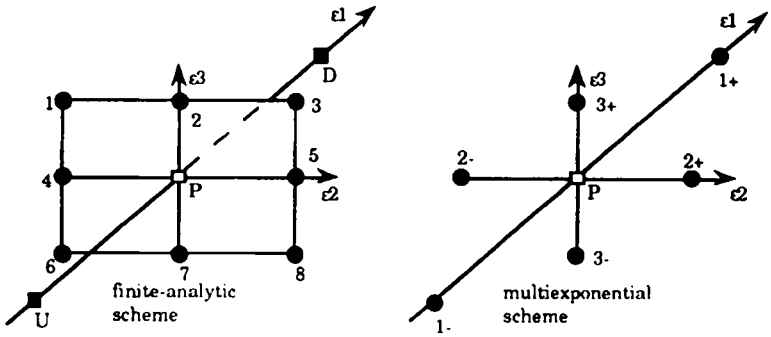

Figure 2

of linear and exponential functions. If g is assumed to be constant on the grid, the analytical solution is

$$\Phi_p = \sum_{i=1}^{8} C_i \Phi_i - C_p g. \tag{13}$$

If S_Φ is assumed to be constant on each grid net, the second equation can be solved like a first-order linear differential equation with constant coefficient. The unknown is Φ_{ε^1} and on a monodimensional grid net the following equation is obtained:

$$(C_u + C_d)\Phi_p - C_u \Phi_u - C_d \Phi_d = g - S_\Phi - D\Phi_t. \tag{14}$$

If a non-centred first-order-accurate discretization of unsteady terms is used, the association of the two equations produces a discretization of the transport equation of the mean momentum on an 11-node spatial grid and two-node temporal grid:

$$\left(1 + C_p(C_u + C_d) + C_p \frac{D}{\tau}\right)\Phi_p = \sum_{i=1}^{8} C_i \Phi_i + C_p\left(C_u \Phi_u + C_d \Phi_d + \frac{D}{\tau}\Phi_p^{n-1} - S_\Phi\right). \tag{15}$$

Nevertheless, this method of discretization requires a lot of CPU time because of the calculation of finite analytic scheme coefficients. Calculation of an infinite series with often poor numerical convergence and imperfectly controlled asymptotic developments is needed. One should also note an asymmetry of the discretization which develops a preferential direction of the mesh.

A multiexponential scheme[15,16] (Figure 2) based on a symmetric decomposition by computational space dimension of the transport equation can also be used. The multidimensional operator of the partial derivative system is represented by a set of differential operators. In each direction a linear differential equation is solved and the following is obtained:

$$\Phi_{\varepsilon^i\varepsilon^i} + 2A_i \Phi_{\varepsilon^i} + g_i = 0 \quad \Rightarrow \quad \Phi_{\varepsilon^i\varepsilon^i} - 2A_i \Phi_{\varepsilon^i} = \frac{1}{C_{pi}}(-\Phi_p + C_i^- \Phi_i^- + C_i^+ \Phi_i^+). \tag{16}$$

The discrete equation is

$$\sum_{i=1}^{3} \frac{1}{C_{pi}}(-\Phi_p + C_i^- \Phi_i^- + C_i^+ \Phi_i^+) = S_\Phi + D\frac{\Phi_p^n - \Phi_p^{n-1}}{\tau}. \tag{17}$$

All the coefficients obtained by this method, like the finite analytic coefficients, are positive and will induce a good conditioning of the velocity matrix. The advantages of this seven-point scheme are its simplicity and speed of calculation of coefficients for a weak memory storage. Nevertheless, the numerical diffusion with this scheme is still too important, in particular for high grid Reynolds numbers.

In order to palliate this drawback, the multiexponential scheme can be combined with a second-order-accurate centred finite difference scheme. We continuously switch between the two methods for a grid Reynolds number (A_l-terms) of about two. All the discretization coefficients are calculated according to $C = (1 - f)C_{cfd} + fC_{mu}$, with $f = 0{\cdot}1 + 0{\cdot}9 \exp[(-A_l/1{\cdot}32)^2]$.

This last scheme is used for all the numerical calculations.

3.3. *Pressure–velocity coupling*

At each time step two linear systems have to be solved simultaneously, namely a linear system coming from the transport equation of momentum and a linear system resulting from mass conservation:

$$(E - A)U + GP = f \quad \text{(S1)}, \qquad DU = g \quad \text{(S2)}. \tag{18}$$

U and P are the velocity and pressure vectors respectively at the nodes of the mesh. The velocity matrix consists of a purely diagonal matrix E and a zero diagonal matrix A. G and D are discrete forms of gradient and divergence operator respectively. Source terms and boundary conditions are gathered in the f- and g-vectors.

If the pressure field was previously known, the velocity field could be determined through the solution of system (S1). Unfortunately, the pressure field is unknown and the equation necessary to determine it is obtained by a linear combination of the two systems (S1) and (S2):

$$D(E - A)^{-1}(f - GP) = g. \tag{19}$$

At present the problem stems from the impossibility of solving this system of equations numerically because of an impossibility of storing the matrix $D(E - A)^{-1}G$ and therefore of inverting it for the considered mesh (around 10^5 nodes): $D(E - A)^{-1}G$ is a full matrix and needs at least 800 Gbyte physical memory for its storage, which is not reasonable. The principle adopted in the iterative resolution algorithm SIMPLER is based on the use of E^{-1} as the approximate inverse of $E - A$. The discrete pressure equation becomes

$$(DE^{-1}G)P = DE^{-1}(AU + f) - g. \tag{20}$$

The Patankar SIMPLER algorithm[3] used to solve the continuity and momentum transport equations is the following.

1. Calculate the purely advective velocity field: $U^* = E^{-1}(AU^{k-1} + f)$.
2. Calculate the pressure field at the previous time: $P^{k-1} = (DE^{-1}G)^{-1}(DU^* - g)$.
3. Solve the momentum transport equation: $U^{**} = (E - A)^{-1}(f - GP^{k-1})$.

The divergence of the velocity field U^{**} is not zero and must be corrected by the following two steps.

4. Calculate the pressure correction: $P' = (DE^{-1}G)^{-1}(DU^{**} - g)$.
5. Calculate the corrected new velocity field: $U^k = U^{**} - E^{-1}GP'$.

3.4. Solution of linear systems

The solution of the SIMPLER algorithm imposes the inversion of three linear systems: one on the velocity matrix $E - A$ (step 3) and two on the pressure and pressure correction matrix $DE^{-1}G$ (steps 2 and 4). These matrices are quite sparse and the position of non-zero values can be easily located by using a structured mesh. An iterative method is used to invert these systems.

The inversion of the velocity system is made easier because the analytical schemes (finite analytic or multiexponential) or the finite difference upwind scheme supply positive coefficients which give a digonally dominant and well-conditioned velocity matrix.

The linear systems studied here are not symmetric generally, so an ordinary conjugate gradient algorithm should not be used. The normal equation method, which consists of restoring the symmetry of the system by left multiplying by the transposed matrix, is a solution to this problem, especially because the new matrix of the system is necessarily positive, ensuring the convergence of the method. Unfortunately, the condition number of the new system becomes the square of the initial system and the rate of convergence of the process is slowed down. Therefore, in order to invert the matrix, a biconjugate gradient method will be used, which will preserve the condition number of the system though it will double the size of the matrix. The convergence of this process is not mathematically proved (the new matrix is not always positive), but until now we have never met a velocity matrix for which the biconjugate gradient method would diverge.

The linear systems for pressure and pressure correction are less easily solved. In fact, the diagonal dominance of the matrix cannot be secured, as in the velocity system, and the refined grid, which is necessary for a good description of the velocity profile in the boundary layer without using a wall function, increases considerably the condition number of the system.

The paradox is then the following: the velocity on the boundary layer changes very quickly and is easily computed, but the pressure varies slowly, making it difficult to calculate.

With the free surface boundary condition the convergence is obtained with more difficulty, because the condition number increases gradually during the time steps, together with the displacement of the free surface.

Thus the number of iterations required by a biconjugate gradient method in order to obtain a good solution of the system increases and sometimes the method diverges. Consequently, a preconditioning of the matrix $DE^{-1}G$ is essential, not only to reduce the cost of CPU time but also to create the convergence of the iterative method. The preconditioning method consists of left multiplying the system $Ax = b$ by a matrix M^{-1} in order to decrease the condition number of the new matrix of the system $(M^{-1}A)$ with respect to that of A. Thus we have to solve the following new system: $M^{-1}Ax = M^{-1}b$.

The biconjugate gradient method preconditioned by a matrix M^{-1} consists of carrying out the following operations up to $r_{j_{\max}}/r_0 < \varepsilon$:

$$r_0 = b - Ax_0, \qquad \bar{r}_0 = b - A^{\mathrm{T}}x_0, \qquad p_0 = z_0 = M^{-1}r_0, \qquad \bar{p}_0 = \bar{z}_0 = M^{-\mathrm{T}}r_0,$$

$$\text{for } j = 1 \text{ to } j_{\max}$$

$$\alpha_j = \langle \bar{r}_j, z_j \rangle / \langle p_j, Ap_j \rangle, \qquad x_{j+1} = x_j - \alpha_j p_j,$$

$$r_{j+1} = r_j - \alpha_j A p_j, \qquad \bar{r}_{j+1} = \bar{r}_j - \alpha_j A^{\mathrm{T}} \bar{p}_j,$$

$$z_{j+1} = M^{-1} r_{j+1}, \qquad \bar{z}_{j+1} = M^{\mathrm{T}} \bar{r}_{j+1},$$

$$\beta_j = \langle \bar{r}_{j+1}, z_{j+1} \rangle / \langle \bar{r}_j, z_j \rangle, \qquad p_{j+1} = \beta_j p_j + z_{j+1}, \qquad \bar{p}_{j+1} = \beta_j \bar{p}_j + \bar{z}_{j+1}.$$

If $M = I_d$ (identity matrix), it is clear that there is no preconditioning. $M = A$ is the more effective theoretical preconditioning, but in this case A^{-1} is still to be calculated. The problem consists of determining a matrix M which is a good and easily invertible approximation of A. Consequently, M is written as a classical LU decomposition which copies the A-structure. The decomposition is written in the form

$$M = LU, \qquad L = (l + \Delta)\Delta^{-1}, \qquad U = (u + \Delta), \tag{21}$$

where l and u are the strict lower and strict upper decompositions of A respectively and Δ is a diagonal matrix such that $\text{diag}(M) = \text{diag}(LU) = (2 - \sigma)\text{diag}(A)$ defined by the following recurrence:

$$\Delta_i = \sigma A_{ii} - \sum_{j=1}^{i-1} \frac{A_{ij}A_{ji}}{\Delta_j}. \tag{22}$$

The matrix $M = LU$ is easily invertible by a standard method ($Mx = y \Leftrightarrow Lz = y$ and $Ux = z$). The only remaining problem of this recurrent method is that it is not vectorizable in this respect. Various algorithms are used to vectorize the inversion of a triangular system, e.g. the decomposition in Neumann series. Nevertheless, the vector performance of the computer has to be considered before using these algorithms.

3.5. *Discretization of free surface boundary conditions*

3.5.1. Kinematic condition. Taking into account that h is the free surface elevation, varying only according to the parameters t, ε^1 and ε^2, we can write the kinematic condition in the form

$$\frac{\partial h}{\partial t} + A^1 \frac{\partial h}{\partial \varepsilon^1} + A^2 \frac{\partial h}{\partial \varepsilon^2} - u^3 = 0,$$

$$A^1 = \frac{1}{J} b_1^1(u^1 - v_g^1) + \frac{1}{J} b_2^1(u^2 - v_g^2) + \frac{1}{J} b_3^1(u^3 - v_g^3), \tag{23}$$

$$A^2 = \frac{1}{J} b_1^2(u^1 - v_g^1) + \frac{1}{J} b_2^2(u^2 - v_g^2) + \frac{1}{J} b_2^2(u^2 - v_g^2) + \frac{1}{J} b_3^2(u^3 - v_g^3).$$

The new position of the free surface at the end of each iteration can be computed under this condition. After the discretization of this equation the new free surface elevation is obtained by solving a linear system. In order to avoid system inversion and to reduce CPU time, a non-centred discretization of the spatial derivative terms is used. This method renders the free surface elevation in the form of an explicit recurrent equation, preserving the implicit characteristic of the discretization. It is essential to use an implicit scheme for the discretization of the kinetimatic condition when a very fine mesh is used because of the very small time step enforced near the body by the stability criterion of the explicit discretization.

The velocities on the free surface (useful for A^i-term calculation) are computed using the two dynamic conditions for u^1 and u^2 and solving the continuity equation for u^3.

The $\partial h/\partial \varepsilon^1$ derivatives are discretized with Dawson's upstream four-point scheme in order to reduce the numerical damping introduced by a two-node discretization.

The discrete free surface kinematic condition is

$$\frac{h_{i,j}^k - h_{i,j}^{k-1}}{\tau} + A^1 \sum_{l=0}^{3} C_l h_{i,j+l}^k + A^2(h_{i,j+l}^k - h_{i,j}^k) - u^3 = 0, \tag{24}$$

i.e.

$$h^k_{i,j} = \frac{h^{k-1}_{i,j} + \tau u^3 - \tau A^1 \sum_{l=1}^{3} C_l h^k_{i-l,j} - \tau A^2 h^k_{i,j+l}}{1 + \tau A^1 C_0 - \tau A^2}, \tag{25}$$

where the C_l-terms are the Dawson scheme coefficients with a constant step. The index k refers to the time step and the indices i and j refer to the ε^1- and ε^2-direction respectively. The C_l-coefficients used are the following: $C_0 = \frac{5}{3}$, $C_1 = -\frac{5}{2}$, $C_2 = 1$, $C_3 = -\frac{1}{6}$. To solve the above-mentioned equation, initial conditions at $t = 0$ and boundaries conditions for $\varepsilon^1 = \varepsilon^1_{\min}$ and $\varepsilon^2 = \varepsilon^2_{\max}$ have to be used:

$$h^0_{i,j} = 0 \quad \text{and} \quad h^k_{i,j\min},\ h^k_{i,j\max} = 0 \quad \text{for all } (i,j).$$

It is important to emphasize the numerical difficulties which have been met around the intersection of the free surface with the hull. On the hull the velocity components verify the no-slip condition $u^1 = u^2 = u^3 = 0$ and the contravariant components of the velocity deformation of the calculation space are equal to zero; therefore the components A^1 and A^2 are equal to zero. There is only one solution to prevent the free surface kinemetic boundary condition from degenerating to $\partial h/\partial \varepsilon^2 = 0$ (in this case the free surface do not go up along the hull). This solution is that $\partial h/\partial \varepsilon^2$ becomes infinite so that $A^2 \partial h/\partial \varepsilon^2$ remains finite and not equal to zero. This mathematical singularity cannot be treated numerically, so the free surface elevation on the hull is computed by $\partial h/\partial \varepsilon^2 = 0$.

3.5.2. Dynamic condition. The normal dynamic free surface condition is taken into account by a Dirichlet condition on the pressure, all the terms of the right-hand side being computed at the previous time step. First-order derivatives on the velocities are expressed with a centred finite difference scheme in directions ε^1 and ε^2 and with a non-centred scheme in direction ε^3.

The surface tension term is generally introduced into the computation in order to regularize numerically the free surface elevation. Nevertheless, the mesh refinement in the boundary layer which is used here gives a very unstable calculation of the radius of curvature and induces irregularities on the calculation of the pressure up to the divergence, so the surface tension term is neglected in the calculation.

Moreover, the normal viscous stress on the free surface may be very important in the boundary layer, and when this term is taken into account in the dynamic condition, the calculation of the pressure is not accurate enough for a good convergence. Therefore the dynamic condition is continuously relaxed in the boundary layer so that the normal dynamic condition tends towards the perfect fluid condition on the hull ($Re \to \infty$) and the normal viscous stress is taken into account exactly outside the boundary layer.

The tangential free surface dynamic conditions are introduced in the form of two Neumann conditions on the velocities u^1 and u^2. The developed form of the conditions is

$$\frac{\partial u^1}{\partial \varepsilon^3} = F_{1,1}\frac{\partial u^1}{\partial \varepsilon^1} + F_{1,2}\frac{\partial u^1}{\partial \varepsilon^2} + F_{2,1}\frac{\partial u^2}{\partial \varepsilon^1} + F_{2,2}\frac{\partial u^2}{\partial \varepsilon^2} + F_{2,3}\frac{\partial u^2}{\partial \varepsilon^3} + F_{3,1}\frac{\partial u^3}{\partial \varepsilon^1} + F_{3,2}\frac{\partial u^3}{\partial \varepsilon^2} + F_{3,3}\frac{\partial u^3}{\partial \varepsilon^3},$$

$$\frac{\partial u^2}{\partial \varepsilon^3} = G_{1,1}\frac{\partial u^1}{\partial \varepsilon^1} + G_{1,2}\frac{\partial u^1}{\partial \varepsilon^2} + G_{1,3}\frac{\partial u^1}{\partial \varepsilon^3} + G_{2,1}\frac{\partial u^2}{\partial \varepsilon^1} + G_{2,2}\frac{\partial u^2}{\partial \varepsilon^2} + G_{3,1}\frac{\partial u^3}{\partial \varepsilon^1} + G_{3,2}\frac{\partial u^3}{\partial \varepsilon^2} + G_{3,3}\frac{\partial u^3}{\partial \varepsilon^3}, \tag{26}$$

with

$$K_{i,k} = b_1^k b_1^3 a_{1i} + b_1^k b_i^3 a_{11} + b_2^k b_2^3 a_{1i} + b_2^k b_i^3 a_{12} + b_3^k b_3^3 a_{1i} + b_3^k b_i^3 a_{13},$$
$$L_{i,k} = b_1^k b_1^3 a_{2i} + b_1^k b_i^3 a_{21} + b_2^k b_2^3 a_{2i} + b_2^k b_i^3 a_{22} + b_3^k b_3^3 a_{2i} + b_3^k b_i^3 a_{23}, \qquad (27)$$
$$F_{i,k} = K_{i,k}/K_{1,3}, \qquad G_{j,k} = L_{i,k}/L_{2,3}.$$

It is noted that $\partial u^1/\partial \varepsilon^3$ and $\partial u^2/\partial \varepsilon^3$ can be expressed independently with one of the two conditions mentioned above; nevertheless, the previous test shows a better convergence of the code when $\partial u^i/\partial \varepsilon^3$ is expressed by the continuity of tangential stress in the direction ε^i.

The meshes that have been used are too coarse to show a boundary layer under the free surface. In order to capture a velocity profile under the free surface, the grid at the free surface has to be refined with the same concentration as on the hull. This will multiply excessively the node number and has not been considered up to now.

A new numerical difficulty appears when both no-slip conditions and free surface conditions are taken into account. Indeed, at the intersection with the free surface $\partial u^i/\partial \varepsilon^3 = 0$ and $\partial u^i/\partial \varepsilon^1 = 0$ for $i = 1, 2, 3$ are given by the no-slip conditions, and when these relations are inserted in the tangential dynamic conditions, the following are obtained:

$$\frac{\partial u^1}{\partial \varepsilon^3} = F_{1,2}\frac{\partial u^1}{\partial \varepsilon^2} + F_{2,2}\frac{\partial u^2}{\partial \varepsilon^2} + F_{3,2}\frac{\partial u^3}{\partial \varepsilon^2}, \qquad \frac{\partial u^2}{\partial \varepsilon^3} = G_{1,2}\frac{\partial u^1}{\partial \varepsilon^2} + G_{2,2}\frac{\partial u^2}{\partial \varepsilon^2} + G_{3,2}\frac{\partial u^3}{\partial \varepsilon^2}. \qquad (28)$$

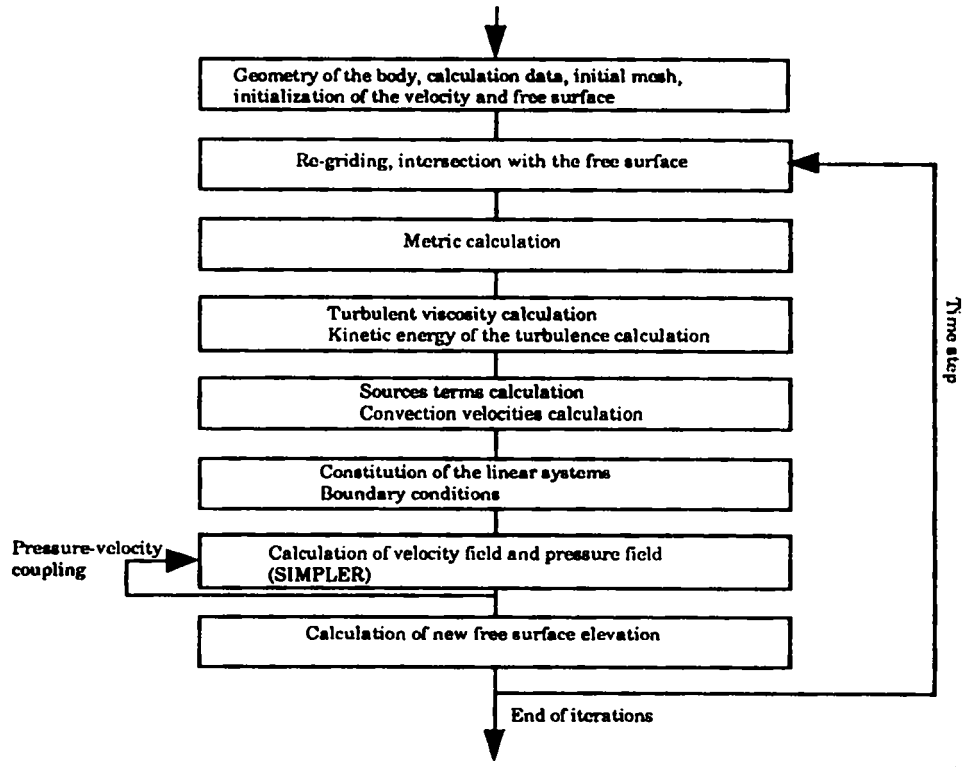

Figure 3

The second member of these equations contains the derivatives of velocities in the ε^2-direction, which is normal at the hull. When these terms are taken into account, an inexorable divergence of the computer code is obtained. The numerical solution consists of suppressing derivatives in the ε^2-direction around the hull at a distance of the magnitude of the boundary layer thickness.

3.6. Organization of computer code

The computer code ELISA based on the above theory is organized according to the chart shown in Figure 3.

4. RESULTS FOR A WIGLEY HULL

The calculation was made around a Wigley hull fixed in heave and pitch. An H-mesh topology has been used on the free surface and a C-mesh topology in the ε^3-direction. The grid used has 41 nodes in the ε^2-direction, 21 in the ε^3-direction and 91 in the ε^1-direction (15 before the hull, 26 behind the hull and 50 along the hull). The whole volume mesh contains 80,000 nodes. The physical space stretches out for one length of the boat above the hull, two lengths behind, one length on the side and half a length under the hull. The first calculation point in the boundary layer is located at $s/l = 0{\cdot}00001$ at the bow and $s/l = 0{\cdot}00005$ at the stern to ensure approximately $y^+ = 3$ for the non-dimensional distance to the body (the refinement of the mesh is varying continuously from the bow to the stern).

The ε^1-direction is the main direction of the flow, the ε^2-direction is normal at the hull surface and the ε^3-direction is parallel to the hull sections from the free surface to the symmetry plane ($\varepsilon^2 = 0$ is the surface which contains the hull, $\varepsilon^3 = 0$ is the free surface equation at each time).

A partial view of the mesh on the bow is shown on Figure 4(a). Figure 4(b) shows the deformation of the mesh of the free surface at the end of the calculation.

The characteristic establishment time of the profile velocity in the boundary layer on the one hand and of the free surface position on the other hand are very different (the total process convergence being ruled by the convergence of the free surface). Thus a constant and uniform time step is used and the iteration is carried until the convergence of the free surface.

A non-dimensional constant time step has been used: $\tau = v_a t/l = 0{\cdot}01$. Iterations have been made till $T = 5$ for high Froude numbers ($Fn > 0{\cdot}35$) and till $T = 10$ for low Froude numbers ($0{\cdot}22 < Fn < 0{\cdot}35$), i.e. 500 or 1000 iterations in 10 or 20 h CPU time on a CRAY2 mono-processor.

Starting the calculation with the final speed of the boat is physically the same as suddenly introducing a hull in a water-circulating channel. A shock is created on the free surface and this requires an important sub-relaxation of the velocity field and free surface elevation to converge. In order to obtain at each time step a physical comparison, the calculation simulates a uniform acceleration to reach the speed wanted.

The unsteady speed of the boat is computed according to $v/v_a = \min(1, aT)$. Therefore we have a first period of time with a constant non-dimensional acceleration a and then a second period of time with a constant non-dimensional speed v/v_a equal to unity. Acceleration terms for the moving system in rectilinear translation are taken into account in the source terms S_Φ. The convergence and the suppression of the relaxation coefficients on the free surface elevation and on velocities are ensured by this technique, so the results of each iteration correspond to a physical unsteady state.

Figure 5 shows a convergence of about third order on velocity, pressure, free surface elevation and pressure integration force. The remaining terms are calculated according to

$$rv = \log\{\max[(v^j - v^{j-1})/v_a]\}, \qquad rp = \log\{\max[(p^j - p^{j-1})/\rho v_a^2]\},$$

$$rh = \log\{\max[(h^j - h^{j-1})/h^j_{max}]\}, \qquad rpt = \log[(Rpt^j - Rpt^{j-1})/Rpt^j].$$

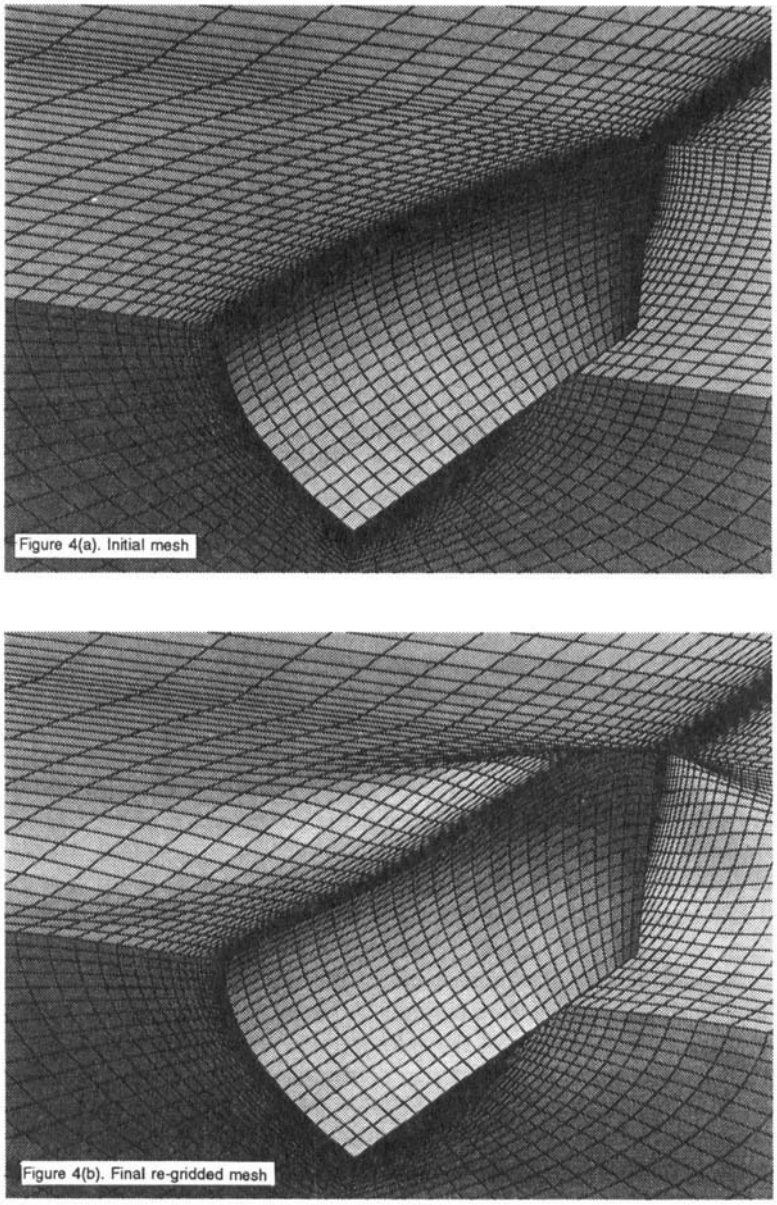

Figure 4.

Figure 6 shows the free surface elevation along the hull (located between $x/l = -0{\cdot}5$ and $x/l = 0{\cdot}5$). Calculations are in good agreement with experimental values at all Froude numbers in spite of a light numerical damping (especially for the lower Froude number of 0·25) which restricts the magnitude of free surface oscillations. Using a finer grid mesh would probably improve the results, in particular the magnitude of the first crest. Viscous effects are visible

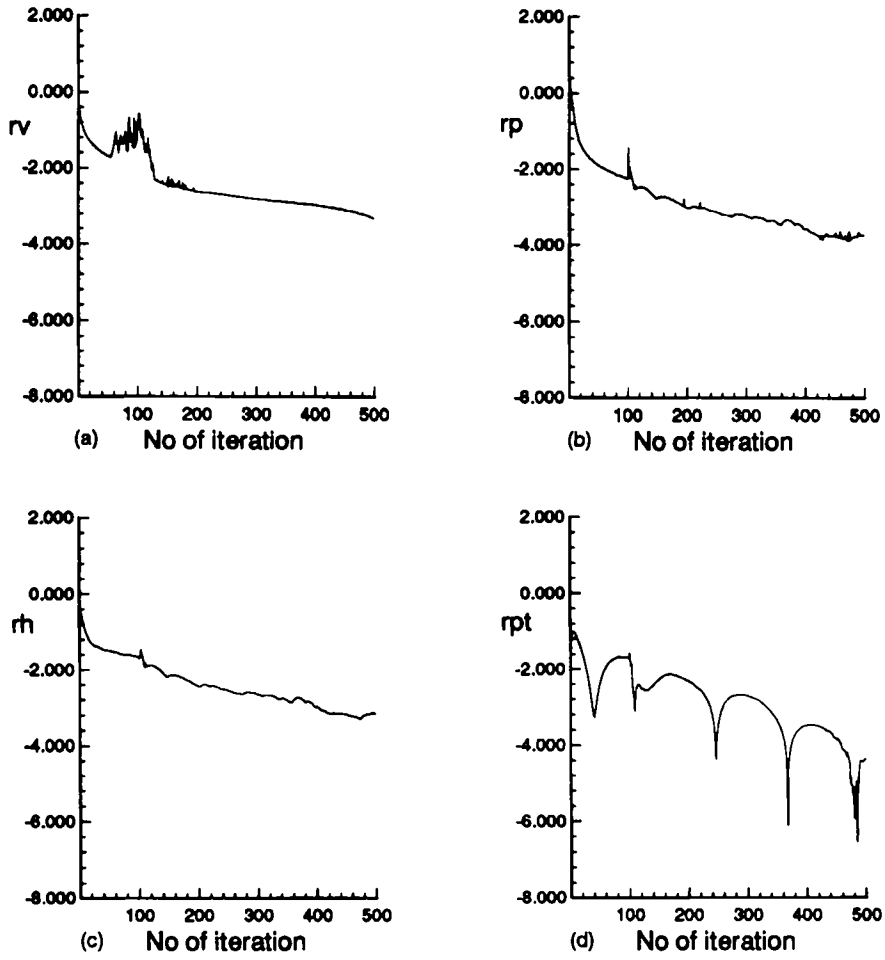

Figure 5. Convergence of (a) velocity, (b) pressure, (c) free surface elevation and (d) pressure integration force

especially on the stern crest; for perfect fluid calculations its amplitude is nearly the same as the bow crest, but in real flows it decreases by about 30%.

Figures 7 and 8 show the calculated and measured[17] velocity profiles in sections $x/l = 0$ and 0·45 respectively. Results for $x/l = 0$ are in accordance with experimental results along the whole section. On the stern of the boat ($x/l = 0{\cdot}45$) the velocity profiles near the free surface are no longer in agreement with experiments. The main difference is that the experimental velocity profiles in the presence of the free surface are very different from the experimental velocity profile for a double-model configuration, but for now all the calculations that have been carried out with the boundary layer approximation or with the Navier–Stokes equations show very little difference between the free surface and double-model calculations for the velocity profile (Figure 8). It is noted that the calculations carried out by Hino[18] (Navier–Stokes) and Stern[10] (boundary layer) give the same conclusions. We suggest two reasons for this phenomenon.

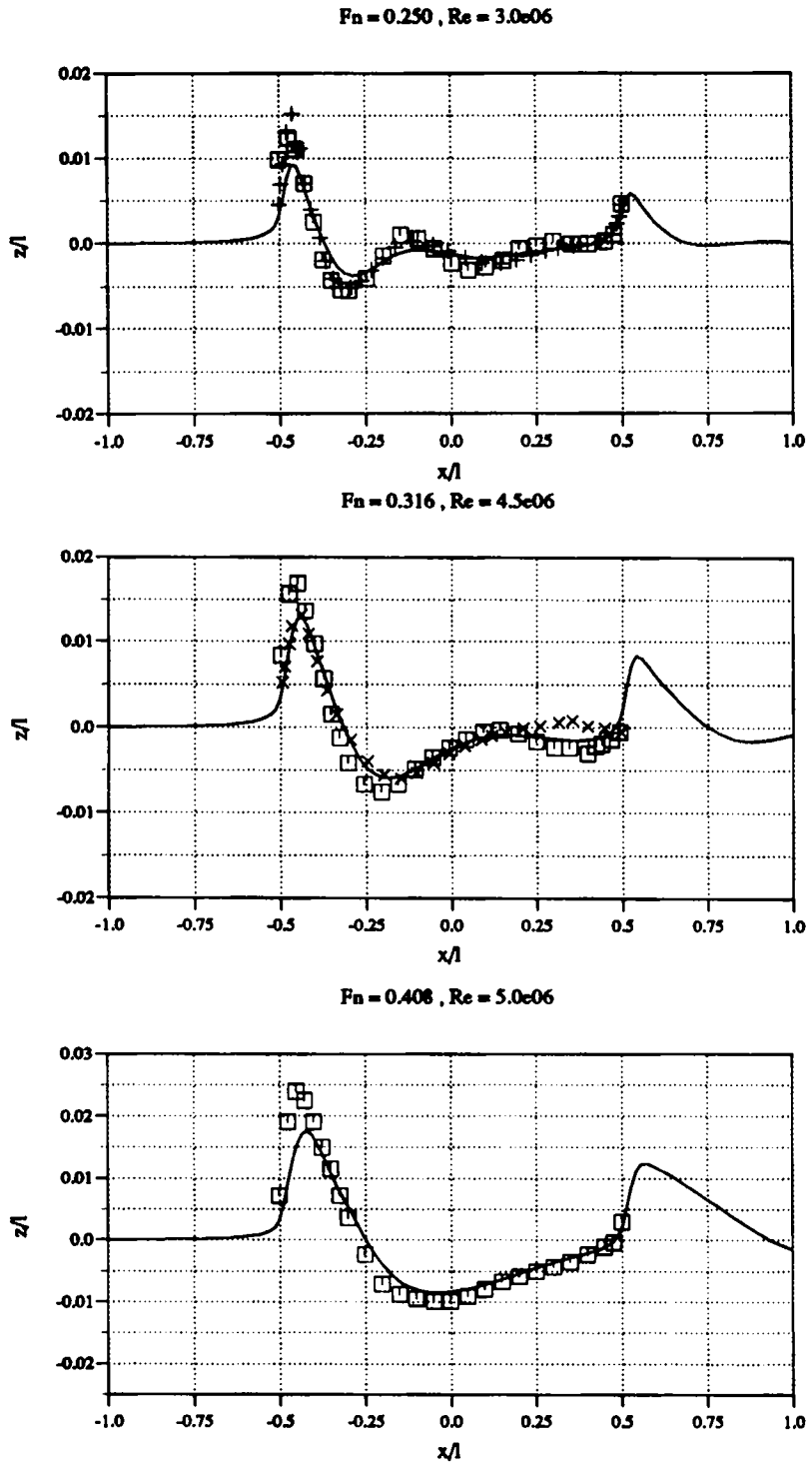

Figure 6. Free surface elevation along the Wigley hull: —, ELISA calculation; ×, Stern calculation; +, Hino calculation; □, experiments

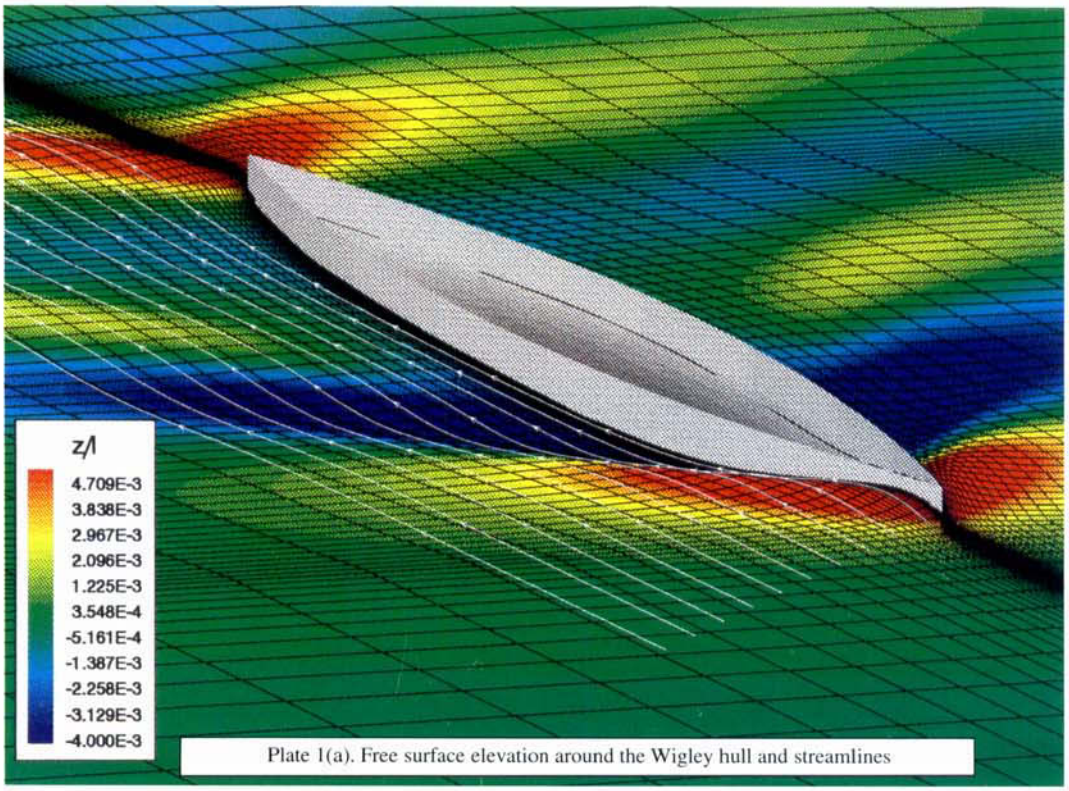

Plate 1(a). Free surface elevation around the Wigley hull and streamlines

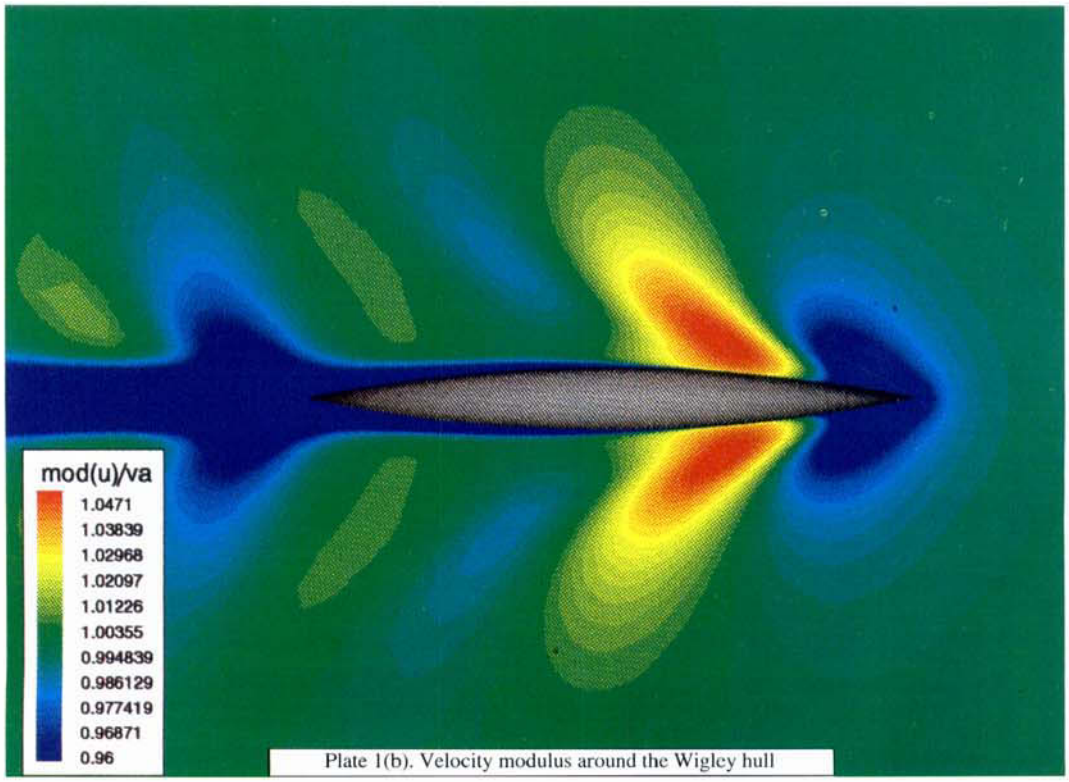

Plate 1(b). Velocity modulus around the Wigley hull

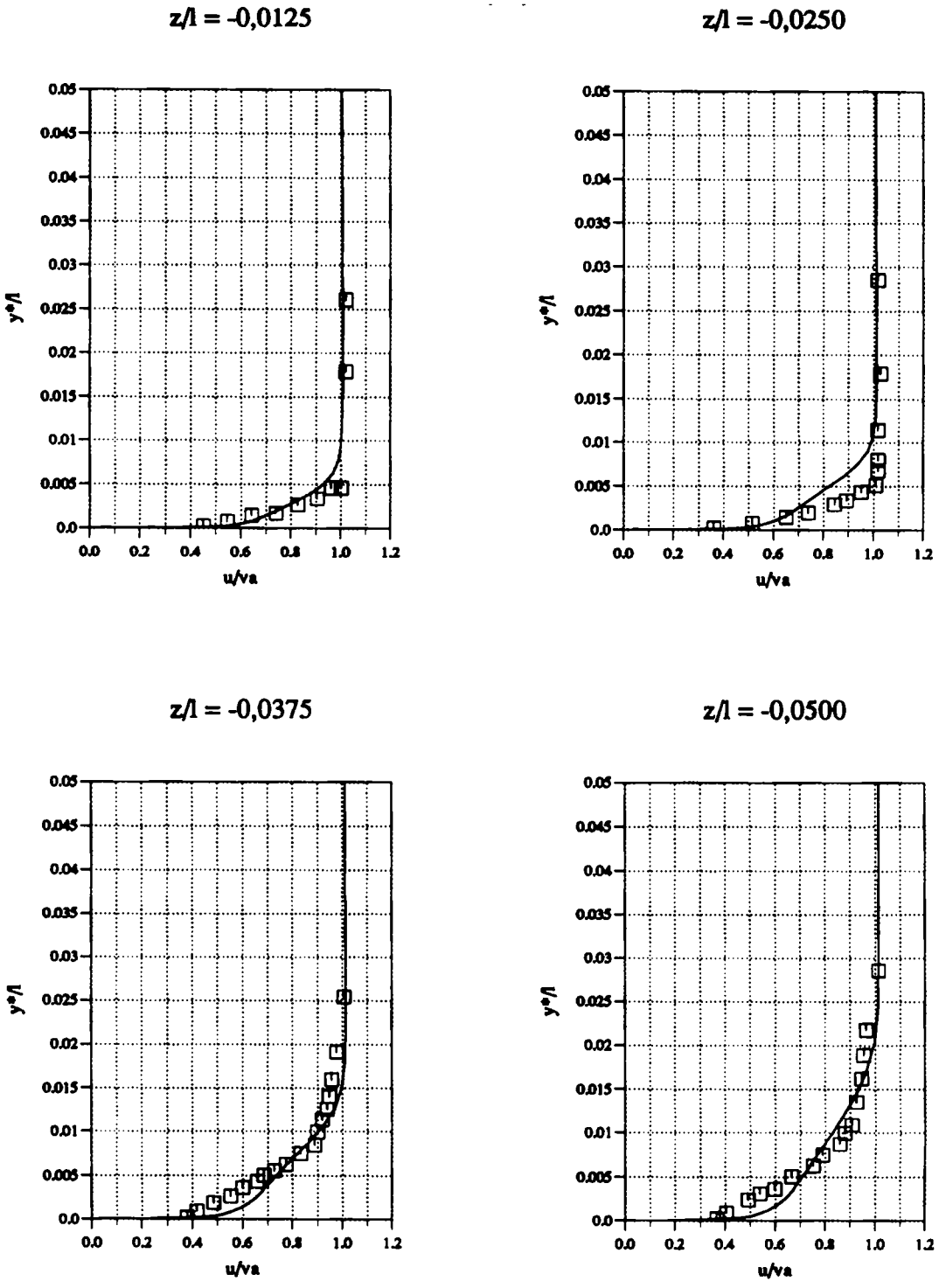

Figure 7. Velocity profiles at $x/l = 0$, $Re = 4{\cdot}5 \times 10^6$ and $Fn = 0{\cdot}316$: —, ELISA calculation; □, Ali experiments

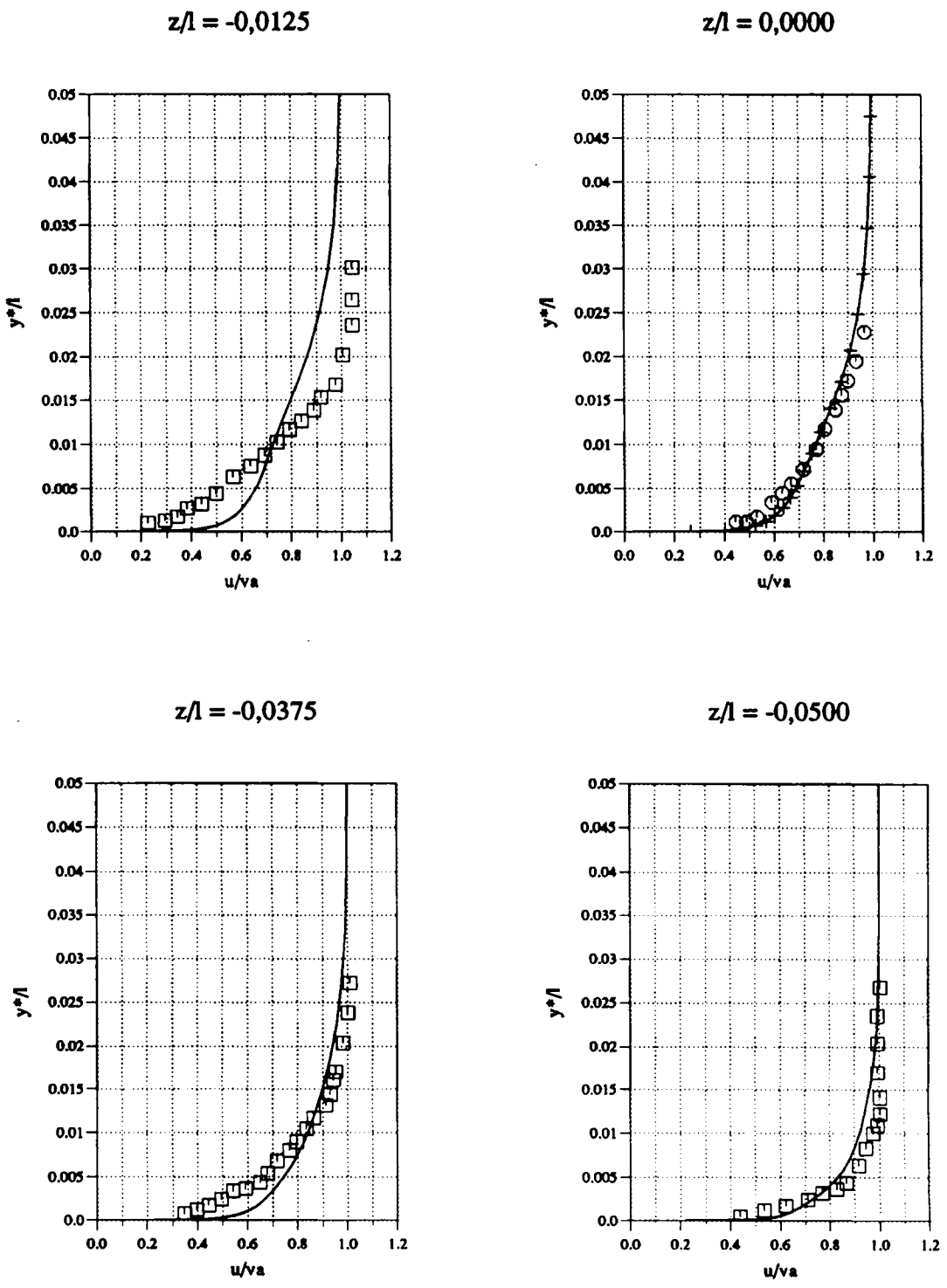

Figure 8. Velocity profiles at $x/l = 0{\cdot}45$ and $Re = 4{\cdot}5 \times 10^6$: —, ELISA calculation ($Fn = 0{\cdot}316$); □, Ali experiments ($Fn = 0{\cdot}316$); +, ELISA calculation ($Fn = 0$); ○, Sarda experiments ($Fn = 0$, $x/l = 0$)

1. Very important modifications in the turbulence characteristics which are not modelized are due to the presence of the free surface.[19] A decrease in the characteristic length of the turbulence and therefore in the turbulent viscosity is observed experimentally and very locally on the free surface. A simplified formulation has been introduced in the Baldwin–Lomax model which consists of calculating the characteristic length no longer as the distance to the wall but as the minimum distance to the wall and to the free surface.[19] Calculations made with this new method indicate that the turbulent viscosity is modified only on a very thin layer under the free surface. This is not enough to explain entirely the differences between experiments and computations.
2. The second hypothesis is related to the implementation of dynamic conditions on the free surface and particularly tangential dynamic conditions which are inconsistent, in the form of Neumann conditions, with the no-slip condition. For this reason the relaxation of the dynamic conditions in the boundary layer is made just where their influence is important. A more exact representation of dynamic free surface boundary conditions would probably improve the calculation of velocity profiles near the free surface.

Plate 1(a) is a three-dimensional colour representation of the initial mesh of the boat and part of the free surface grid. The scalar which is represented on the free surface is the elevation of the free surface, h. We can see in this figure, first, that the grid is fitted to the body and to the unsteady free surface: the hump on the bow of the boat and the following hollow along the hull can be distinctly noticed (the hump on the bow of the boat and the following hollow along the hull can be distinctly noticed (the hump is in red and the hollow in blue). The interaction of the free surface with the boundary layer is shown by a smaller hump on the stern than on the bow. This phenomenon is at the origin of the form resistance which is unreachable by perfect fluid calculation. In Plate 1(a) the free surface streamlines can be seen in white (at the convergence the free surface is a stream surface).

Plate 1(b) shows the distribution of the velocity modulus on the free surface. Free surface effects can be observed: the decrease in velocity on the hump and the increase in velocity on the hollow of the free surface. These effects can also be found in a perfect fluid, since in this case the free surface elevation is proportional to the square of the difference between the modulus of the velocity and the upstream infinite velocity. Viscous effects such as the expansion of the boundary layer are manifested by a decrease in velocity along the hull or a softening of free surface oscillations in the wake. Nevertheless, the excessive mesh stretching in this domain may also be a cause of this softening. More accurate calculation of the free surface elevation downstream of the hull would require a very fine grid in the ε^1-direction (i.e. along the hull), but such a grid would at present increase the CPU time excessively.

All the calculations are realized in unsteady mode and the evolution of the resistance of the boat versus time has been studied.

The total resistance Rt which is computed by the resolution of the free surface Navier–Stokes equation is fundamentally divided into two distinct parts: the tangential frictional resistance Rf which originates from the Newtonian modelization of the viscous stress tensor, and normal pressure forces which result from the total pressure integration on the hull, Rpt. This last component consists of the integration of the dynamic pressure Rpd and of the static pressure Rps. The total pressure integration may also be decomposed into the wave resistance Rw, which is the only resistance in a perfect fluid, and the form resistance Rfo. These different components of resistance are computed according to the following equations, where Rf_i, Rpd_i and Rps_i are the components of the forces in system x^i:

$$Rt = Rf + Rpt, \qquad Rpt = Rpd + Rps = Rw + Rfo$$

$$Rf_i = \int_{\varepsilon_i^3}^{\varepsilon_i^3} \int_{\varepsilon_i^1}^{\varepsilon_i^1} \nu\left(\frac{\partial u^i}{\partial x^j} + \frac{\partial u^j}{\partial x^i}\right) b_j^2 \, d\varepsilon^1 \, d\varepsilon^3, \qquad Rpd_i = \int_{\varepsilon_i^3}^{\varepsilon_i^3} \int_{\varepsilon_i^1}^{\varepsilon_i^1} - pb_i^2 \, d\varepsilon^1 \, d\varepsilon^3,$$

$$Rps_i = \int_{\varepsilon_i^3}^{\varepsilon_i^3} \int_{\varepsilon_i^1}^{\varepsilon_i^1} \rho g x^3 b_i^2 \, d\varepsilon^1 \, d\varepsilon^3 \tag{29}$$

Resistance coefficients are calculated according to $Cx = 2Rx/(\rho SVa^2)$, where S is the static wetted surface.

Figure 9(a) shows the evolution of the total pressure integration versus time for two Froude numbers, $Fn = 0{\cdot}250$ and $0{\cdot}316$, for the same initial non-dimensional acceleration $a = 1 = Al/Va^2$, where A is the dimensional acceleration and Va is the speed of the boat. The appearance of resistance oscillations after the acceleration slope for both Froude numbers can be noted, but the convergence of the resistance is faster for the highest Froude number: the pressure integration is converged for $T = 5$ at $Fn = 0{\cdot}316$ and at $T = 10$ for $Fn = 0{\cdot}250$. These oscillations of resistance after an acceleration slope may be observed during towing tank tests; moreover, Wehausen has studied this phenomenon analytically on a cylinder under the free surface for an irrotational flow in a perfect fluid (potential flow). The decomposition of the two first-order terms of resistance displays the oscillation of the resistance with a period t_0 according to $2\pi Va/gt_0 = \frac{1}{4}$, which gives in non-dimensional variables $T_0 = 8\pi Fn^2$, where $T_0 = t_0 Va/l$.[20] This formulation of the oscillation period is in good agreement with the calculation presented in Figure 9(a). It is important to note also that the converged values of both resistances are in accordance with towing tank experiments.

It is shown in Figure 9(a) that the convergence of the solution for high Froude numbers is faster than for small Froude numbers; moreover, the free surface elevation is almost converged when the pressure integration is still oscillating. Consequently, it is more difficult for a given Reynolds number to obtain the steady solution for small Froude numbers, not only because of the slower time convergence but also because the capture of the small wavelength on the free surface elevation requires a finer free surface grid. Therefore it has been tried to reduce the convergence time for small Reynolds number by decreasing the initial acceleration. This figure also shows the frictional resistance (for the two Froude numbers we obtain two superposed curves). It is noted that this component of the resistance converges faster than the pressure integration and does not present oscillations like it. (The coupling of the frictional component with the free surface is weak.) The converged value of the frictional resistance is in good agreement with the ITTC 57 formula.

Figure 9(b) shows the result of the pressure integration for two non-dimensional accelerations. It can be seen that for the small acceleration ($a = 0{\cdot}4$) the first peaks are smaller than for the large acceleration ($a = 1$) but the total convergence duration is the same.

It has to be noted the good agreement of the pressure integration resistance with experimental values in spite of the damping of the free surface first creast, but we can observe the same results for the calculation of wave resistance with a potential flow formulation.[1,2] Concerning the viscous resistance, the calculation is more sensitive to the position of the first point in the boundary layer than to the grid size.[21] A finer grid ($101 \times 41 \times 31$) with the same body concentration gives almost the same numerical results (within 1%). Moreover, the calculation of the viscous resistance on the Wigley hull is confirmed by the utilization of a logarithmic law for $y^+ = 100$.

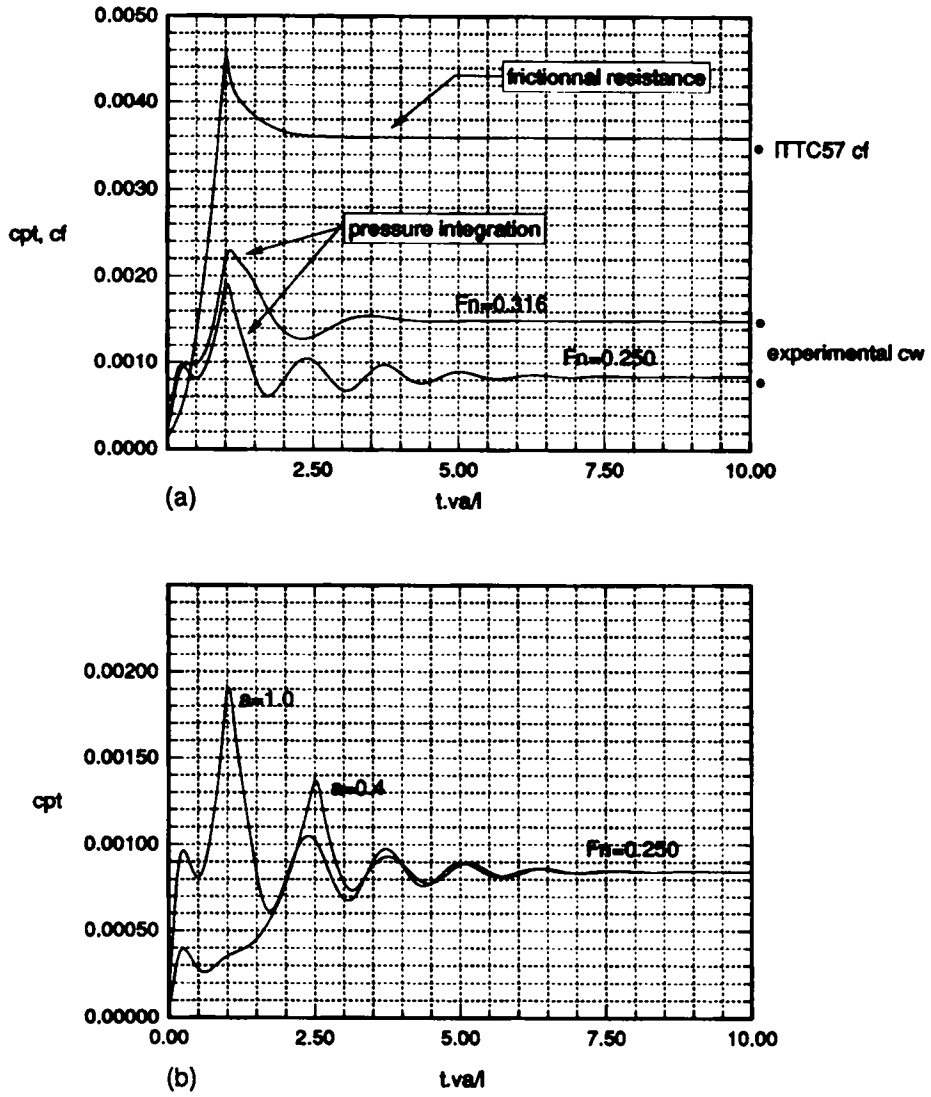

Figure 9. (a) Pressure integration and frictional resistance at $Re = 4{\cdot}5 \times 10^6$. (b) Pressure integration at $Re = 4{\cdot}5 \times 10^6$ for two accelerations

5. CONCLUSIONS

The study which has been presented in this paper should prove the ability of a computer code to solve three-dimensional unsteady incompressible Navier–Stokes equations which take into account fully non-linear boundary free surface conditions. The software can take into account all kinds of hulls which can be meshed by an H-topology in the intersection with the free surface and which have a symmetry with the $x^1 0 x^3$ plane.

The results obtained for a Wigley hull advancing on initially calm water are satisfactory, though the mesh may be too coarse at present to compute all the oscillations of the free surface at small Froude numbers. A more complex hull such as a series 60 hull may require a finer grid

to obtain converged velocities and pressure field. Some calculations on this model, which present strong interactions between the boundary layer and the exterior zone at the stern, will be considered.

Nevertheless, a few critical problems have not be solved up to now.

1. The modelization of turbulence near the free surface is a problem which has not yet yielded entirely satisfactory solutions.
2. Obtaining a better solution for velocity profiles near the free surface is certainly linked to a better consideration of the dynamic free surface condition, the effects of which are important in the boundary layer.

REFERENCES

1. G. Delhommeau, 'Les problèmes de diffraction-radiation et de résistance de vagues: étude théorique et résolution numérique par la méthode des singularitiés', *Thèse de Doctorat ès Sciences*, LHN, ENSM, Nantes, 1987.
2. J. J. Maisonneuve, 'Résolution du problème de la résistance de vagues par une méthode de singularités de Rankine', *Thèse de Doctorat*, LHN, ENSM, Nantes, 1989.
3. J. Piquet and M. Visonneau, 'Computation of the flow past shiplike hull', *Comput. Fluids*, **19**, (1991).
4. V. C. Patel, H. C. Chen and S. Ju, 'Ship stern and wake flow: solution of the fully elliptic Reynolds averaged Navier–Stokes equations and comparisons with experiment', *HHR Report*, no. 323 (1988).
5. M. Zhu, H. Miyata and H. Kajitani, 'Finite difference simulation of a viscous flow about a ship in arbitrary configuration', *Proc. 5th Int. Conf. on Numerical Ship Hydrodynamics*, Hiroshima, 1989.
6. F. Villeger and B. Alessandrini, 'Interaction between free surface flow and boundary layer around a ship model', *Proc. 7th Workshop on Water Waves and Floating Bodies*, Val de Reuil, 1992.
7. H. Miyata, M. Zhu and O. Watanabe, 'Numerical study on a viscous flow with free surface waves about a ship in steady straight course by a finite-volume method, *J. of Ship Res.*, **36**(4), (1992).
8. Y. Yamada and H. Miyata, 'A finite-difference method for a separating flow past a body of arbitrary geometry in rectangular coordinate systems', *Meeting of the Soc. of Nav. Archit.*, 1990.
9. V. Dussan, 'On the spreading of liquids on solids surfaces: static and dynamic contact lines', *Ann. Rev. Fluid Mech.*, **11**, (1979).
10. F. Stern, 'Effects of waves on the boundary layer of surface piercing body', *IIHR Reprot*, no. 288 (1985).
11. R. S. Baldwin and H. Lomax, 'Thin layer approximation and algebraic model for separated turbulent flows', *16th AIAA Meeting*, 1978.
12. L. E. Erikson, 'Generation of boundary conforming grids around wing-bodies configuration using a transfinite interpolation', *AIAA Journal*, **20**, (1982).
13. C. J. Chen and H. C. Chen, 'Finite analytic numerical method for unsteady twodimensional Navier–Stokes equations', *J. Comput. Phys.*, **53**, (1984).
14. C. J. Chen and H. C. Chen, 'The finite analytic method', IIHR Report, no. 232 (1982).
15. G. Deng, 'Résolution des équations de Navier–Stokes tridimensionnelles. Application au calcul d'un raccord plaque plane-aile', *Thèse de Doctorat*, GMN, LHN, ENSM, Nantes, 1989.
16. P. Queutey, 'Résolution des équations de Navier–Stokes tridimensionnelles. Application au calcul sur des corps en incidence', *Thèse de Doctorat*, GMN, LHN, ENSM, Nantes, 1989.
17. Y. Tahara, F. Stern and B. Rosen, 'An interactive approach for calculating ship boundary layer and wakes for non zero Froude number', *J. Comput. Phys.*, **98**, (1992).
18. T. Hino, 'Numerical simulation of a viscous flow with a free surface around a ship model', *J. Soc. Naval Architect. Jpn.*, **161**, (1987).
19. I. Celik, W. Rodi and M. S. Hossain, 'Modelling of free surface proximity effects on turbulence', *Proc. Refined Modelling of Flows*, Paris, 1982.
20. J. V. Wehausen and E. V. Laitone, 'Surface waves', *Handbuch der Physik*, Band IX, Strömungsmechanik III, Springer-Verlag, Berlin, 1960, pp. 446–815.
21. L. Larsson, V. C. Patel and G. Dyne, (eds.) 'Ship viscous flow' in *Proceedings of 1990 SSPA-CTH-IIHR Workshop*, Flowtech International AB, Gothengurg, 1991.
22. S. Chiba and K. Kuwahara, 'A finite difference formulation for free surface flow problems using a conforming grid system', *Proc. 12th Int. Conf. on Numerical methods in Fluid Dynamics*, Oxford, 1990.
23. A. Jenning and G. A. Malik, 'The solution of sparse linear equations by conjugate gradient method', *Int. j. numer. methods eng.*, **12**, (1977).